changing exhaust gas temperature of the helicopter engine [7]. It was observed that surface having a low skin emissivity will be better at suppressing radiation for any particular exhaust temperature. The mixing capacity, effectiveness of a lobe ejector along with double wall diffuser was studied [8]. They studied the effects of ratio of area of the primary flow and that of the secondary flow and the effect of speed of primary flow on the ejection flow ratio rate. They also studied the ejection flow rate ratio from the gap of double wall as well as the mixing velocity distribution.

Effect on heat transfer by an impinging jet on a non-uniform heated plate was studied by Casanova and Ortiz [9]. Their major field of study was whether the variation of the surface geometry has any effect on the heat transfer or not. A studied the effect of cross flow on heat transfer on a protruded surface [10]. They used nano-fluid jet which was impinged normal to plate surface. They concluded that higher the number of protrusions, the better it is for effective heat transfer. A conducted similar study on the protruded surfaces [11-12]. A studied the entrainment of air in a louvered straight funnel [2-4]. The effect of opening area and the quantity of the louvers along with variation in mass suction due to change in funnel configuration were studied. They concluded that mass entrainment increased with increase in area of louvers.

However, the numbers of the louvers had negligible effect on the mass entrainment. They also suggested that keeping the louvers near the nozzle entry point and having open funnel bottom area gives a better entrainment in case of straight funnel. A used a downsized model to study the entrainment through a straight louvered funnel [1,2]. A studied the effect of both hot and cold nozzle exit fluid on mass entrainment in a scaled down IRS device [1,3,13,14]. An empirical equation for the calculation of mass entrainment ratio was also given [15]. In all the above studies, the effect of flowing wind on the mass suction was not reported. An attempt has been made in this study to numerically investigate the effect of cross flow of wind on the mass suction through a louvered funnel.

3. MATHEMATICAL FORMULATION

The problem was solved using a k- ε model [16]. For the k-ε model, the continuity equation is:

$$\frac{\partial \rho}{\partial t} + \frac{\partial(\rho U_j)}{\partial x_j} = 0$$

(1)

The momentum equation is:

$$\frac{\partial \rho U_i}{\partial t} + \frac{\partial}{\partial x_j}(\rho U_i U_j) = -\frac{\partial p'}{\partial x_i} + \frac{\partial}{\partial x_j}\left[\mu_{eff}\left(\frac{\partial U_i}{\partial x_j} + \frac{\partial U_j}{\partial x_i}\right)\right] + S_M$$

(2)

Where, $\mu_{eff} = \mu + \mu_t$

$$\mu_t = C_\mu \rho \frac{k^2}{\varepsilon}$$

(3)

The relation between turbulence viscosity and turbulence kinetic energy as assumed in a k-ε model is shown in equation (3).
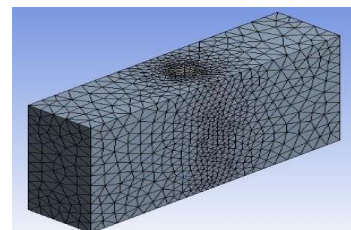
4. COMPUTATIONAL MODEL

Conservation equation of mass/continuity equation, momentum equation, transport equations for turbulent kinetic energy (k) and transport equation for dissipation rate of turbulent kinetic energy (ε) has been integrated over a control volume using finite volume technique. The volume was meshed using tetrahedral elements and FEA tool was used for

solution. The Standard k- ε model with scalable wall function was used for solution. The mass suction ratio was computed for this study. Initial solution was run on first order upwind scheme and then a higher order scheme was used for better accuracy. Mesh independence study for the model was done. The results are reported in Figure 1. Above 2,40,000 elements the negligible variation (within 2%) was observed. The denser the mesh, higher the accuracy, but it would increase computational time.

For using a standard k- ε model, Y^+ above 30 is required. So the model was meshed using ~ 2,70,000 elements (Figure 2), with refined mesh at the louvers, funnel wall near louvers (Figure 3) and the nozzle inlet.
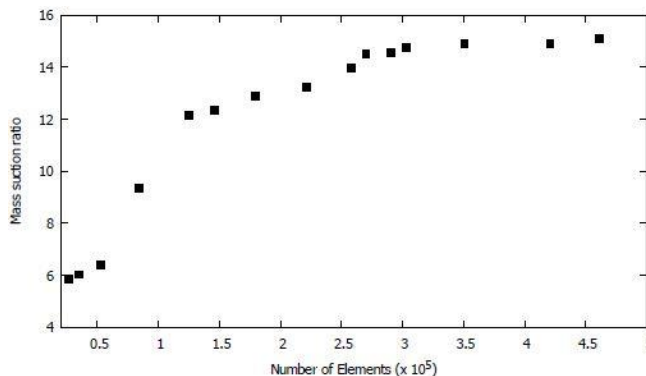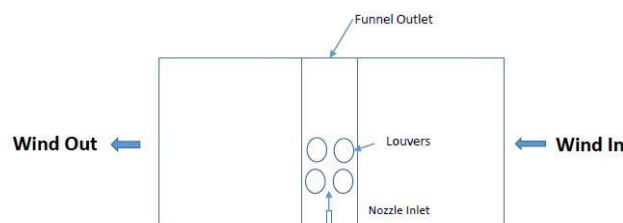

Figure 1: Mesh Convergence

Figure 2: Overall Mesh
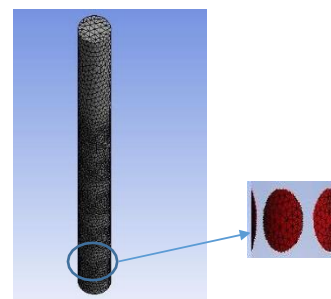
Figure 3: Funnel & Louvers Mesh

5. BOUNDARY CONDITIONS

The details of the boundary conditions can be found in Figure 4.

Figure 4: Boundary Conditions

The computational domain has been given a velocity inlet condition in the "wind in" face (Figure 4) and pressure outlet condition in "wind out" face (Figure 4). Wind velocity has been assumed till 20 m/s for study purpose. The remaining faces of the computational domain was given no slip no shear wall condition. Velocity inlet was given for fluid flow at nozzle entry. The nozzle and funnel wall was given a no-slip; no shear

wall condition. Funnel exit was given a pressure outlet boundary condition. The turbulent intensity ratio has been set at 2% at all velocity inlet conditions and 5% for all pressure outlet condition. The working fluid for this study is air. The nozzle diameter is 0.0125 m and the ratio of funnel diameter to nozzle diameter (D_f/D_{nz}) is kept 11.2. For the first case of study the funnel has been subjected to wind velocity till 20 m/s with louvers kept symmetrical to central axis of funnel and diameter of the louvers are kept as maximum as geometrically possible. In the second study the diameter of the louvers has been reduced the angular distance between the louvers is varied.

6.   VALIDATION OF EXPERIMENTAL RESULTS WITH CFD

The experimental results were used for validation with simulation results for gaining confidence in the software as well in the simulation procedure [1]. A comparison study is shown in the below sections.

6.1   Effect on the mass suction ratio due to change in Reynolds number

The mass suction ratio was calculated by increasing the nozzle exit Reynolds number. Figure 5 shows the comparison between the experimental results and current simulation results. The results conform with each other and a linear variation can be seen between mass suction ratio and increasing Reynold number. However, the variation in the overall value of mass suction ratio is negligible.
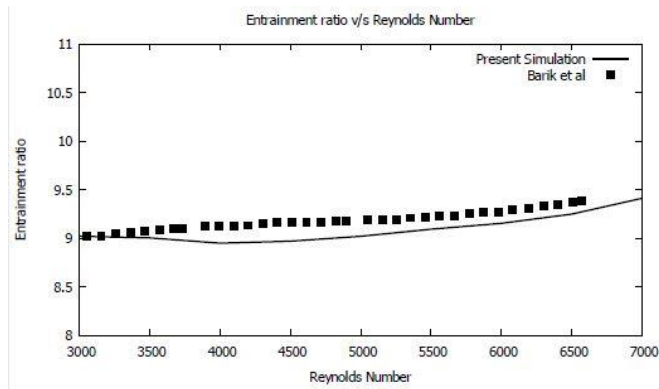

Figure 5: Mass suction ratio v/s Reynolds number

6.2   Effect on mass suction ratio with nozzle protrusion length (L_p)

The protrusion of the nozzle inside the funnel was varied and its effect on the mass suction ratio was calculated. The length by which a nozzle is inserted inside the funnel is known as nozzle protrusion length. The mass suction keeps increasing up to protrusion ratio of 8. Beyond 8, change is negligible. As the nozzle exit move towards the top row of louvers the mass suction ratio becomes almost constant as can be seen in case of protrusion length of 8 to 12.
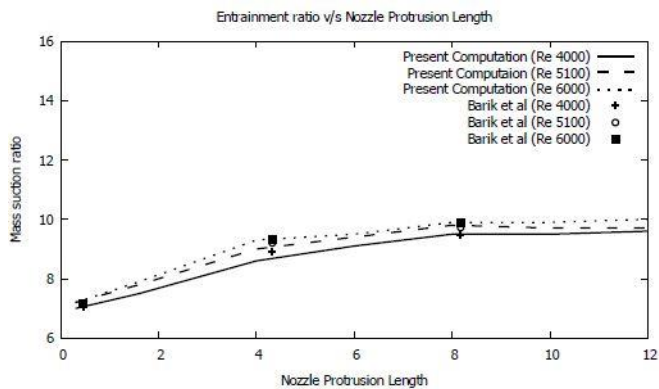

Figure 6: Mass suction ratio v/s nozzle protrusion length

6.3   Effect on the mass suction ratio with change in the total louver

area

The variation in the mass suction ratio with change in louvers opening area was calculated. Increasing the area increased the mass suction ratio and vice versa. The comparative study is reported in Figure 7. The computation for validation purpose was done for two different nozzle exit fluid temperatures. The term temperature ratio in the below graph is the ratio of nozzle fluid exit temperature and the surrounding atmospheric temperature (T_{nz}/T_{sur}).
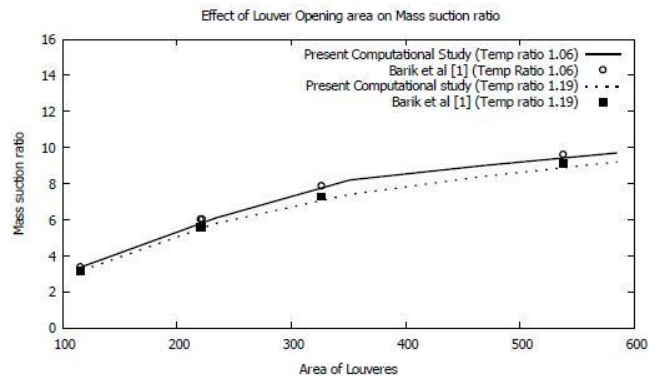

Figure 7: Mass suction ratio v/s louver opening area

7.   RESULTS & DISCUSSION FOR CURRENT STUDY

In the present study the conditions of external fluid flow have been simulated and its effect on the mass suction ratio has been analyzed. In addition to this the effect of exhaust flow parameters, structural changes like hole placement, varying angular distance between holes on mass suction ratio has been studied.
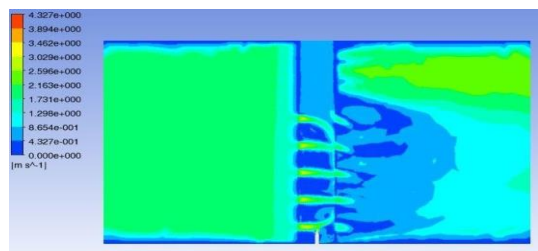

Figure 8: Velocity Plot: Re= 3000, Wind Velocity 2 m/s

The velocity plot in Figure 8 above, shows the flow pattern at the entrance of the louvers, the nozzle exit and the overall computation domain. The increase in velocity near the louvers area can be seen from the contour plot. The dark area between two consecutive rows of louvers shows lower velocity because the fluid got entrapped between the incoming high velocity fluid from the louvers. The high velocity nozzle exit fluid and the incoming surrounding fluid through the louvers strike with each other orthogonally, as a result of which both the fluids loses their kinetic energy. This is evident by the contour color at the IRS funnel exit that represents the velocity after mixing.

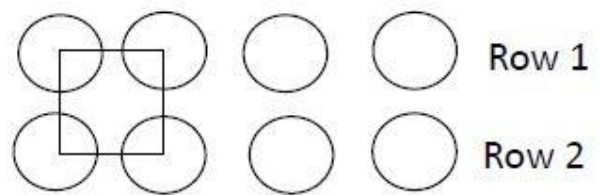### 7.1 Flow computation for rectangular placement of louvers.

Figure 9: Rectangular placement

The effect of the wind velocity was computed for above shown rectangular arrangement of louvers. Figure 9 shows the arrangement of two consecutive rows of louvers on the funnel wall. In the sub-sections below the effect on the mass suction ratio due to changing Reynolds number of

the nozzle exit fluid and that with the wind velocity is reported.

7.1.1 Effect of Nozzle exit Reynolds number

The Reynolds number (Re) of the nozzle exit fluid was varied in the range of $3000 \leq R \leq 7000$ and the mass suction ratio was computed for different wind velocities as shown in Figure 10. Mass suction ratio shows a linear variation with the increasing Reynolds number, but with the increase in the Reynolds number of the nozzle exit fluid, the mass suction ratio through the louvers decreases. This is true for all wind velocities. This might be due to the fact that as we increase the inlet velocity the turbulence at the entry points near the hole increases owing to less mass entrainment. Also, at lower Reynolds number, the difference between the mass suction for higher wind velocity and the next lower wind velocity is higher as compared to a similar situation for higher nozzle exit Reynolds number. This may be due to the reason that lower Reynolds number provides less turbulence for mass suction which accounts for the higher mass suction ratio as compared to that of high Reynolds number.
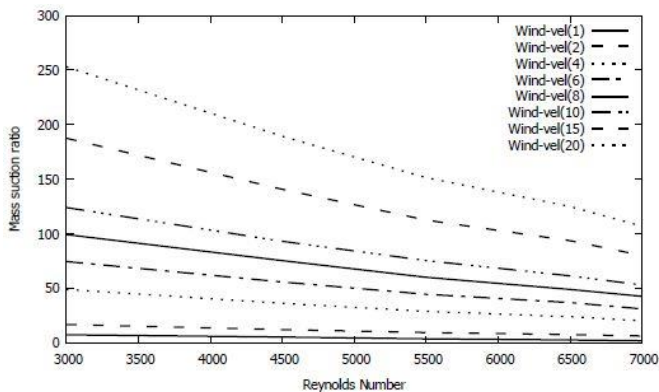

Figure 10: Effect on Mass suction ratio with Reynolds number for different wind velocity

7.1.2 Variation of mass suction ratio with Wind velocity

The change in the mass suction ratio with the change in wind velocity is shown in Figure 11. As we increase the wind velocity, the mass suction ratio keeps on increasing and shows a linear trend. Each curve on the graph represents a different Reynolds number. The variation is similar across all Reynolds number. As we increase the nozzle exit Reynolds number, the mass suction ratio increases. With the increasing wind velocity, the difference between the mass suction ratio between two consecutive Reynolds number keeps on increasing. Also, for the lower Reynolds number the mass suction ratio is higher as compared to that for a higher Reynolds number. This may be due to the reason that lower Reynolds number provides less turbulence for mass suction which accounts for the higher mass suction ratio as compared to that of high Reynolds number This can be seen from the graph's diverging trend.
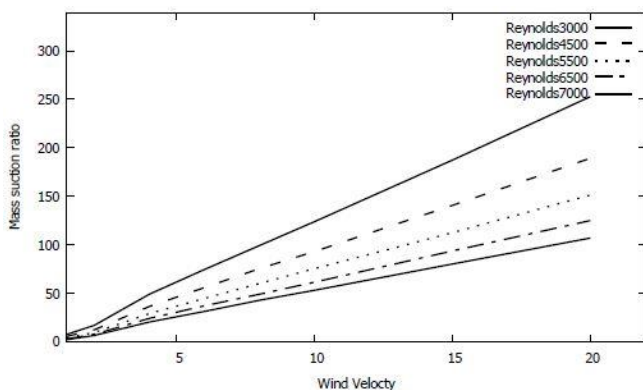

Figure 11: Variation of mass suction ratio with wind velocity for different Reynolds number

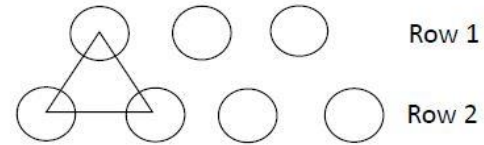### 7.2 Flow computation for triangular placement of louvers

Figure 12: Triangular placement

In Figure 12 triangular placement of louvers is shown. In this arrangement the louvers in row1 is placed in between the two consecutive louvers in the row2. In the section below, the variation of the mass suction ratio with Reynolds number of the exhaust fluid and that with the wind velocity is shown.

7.2.1 Effect of nozzle exit Reynolds number.

The Reynolds number (Re) of the nozzle exit fluid was varied in the range of $3000 \leq R \leq 7000$ and the mass suction ratio was computed for different wind velocities as shown in Figure 13. Mass suction ratio shows a linear variation with the increasing Reynolds number, but with the increase in the Reynolds number of the nozzle exit fluid, the mass suction through the louvers decreases. This may be due to the fact that, as we increase the inlet velocity the turbulence at the entry points near the louvers increase resulting in less mass suction. Also at lower Reynolds number, the difference between the mass suction for higher wind velocity and the next lower wind velocity is higher as compared to a similar situation for higher nozzle exit Reynolds number. This may be due to the reason that lower Reynolds number provides less turbulence for mass suction which accounts for the higher mass suction ratio as compared to that of high Reynolds number.
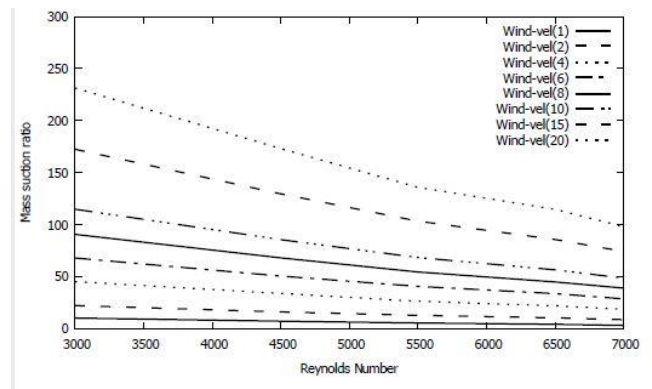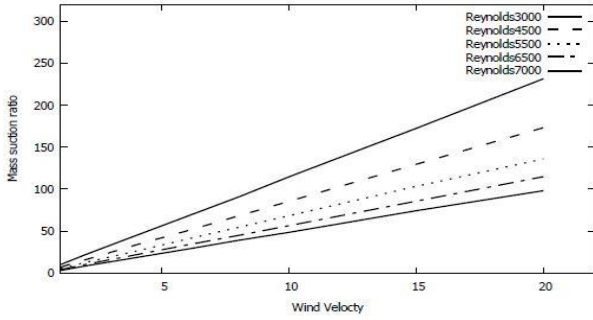

Figure 13: Effect on Mass suction ratio with Reynolds number for different wind velocity

7.2.2 Variation of mass suction ratio with Wind velocity

The change in the mass suction ratio with the change in wind velocity has been computed. As we increase the wind velocity, the mass suction keeps on increasing and shows a linear trend. The variation at different Reynolds numbers is represented by the curves in the graph. It can be seen from the graph that at lower wind velocity, the change in the mass suction ratio shows a linear trend trend. However, as we keep increasing the wind velocity, the mass suction ratio keeps on increasing.

As we increase the nozzle exit Reynolds number, the mass suction ratio increases. With the increasing wind velocity, the difference between the mass suction ratio between two consecutive Reynolds number keeps on increasing. Also, for the lower Reynolds number the mass suction ratio is higher as compared to that for a higher Reynolds number. This may be due to the reason that lower Reynolds number provides less turbulence for mass suction which accounts for the higher mass suction ratio as compared to that of high Reynolds number. This can be seen from the graph's diverging trend.

Figure 14: Variation of mass suction ratio with wind velocity for different Reynolds number

7.3 Flow computation by varying the angle between the louvers.

In this computation, the angle between the adjacent louvers in a row is varied to see the effect on the mass entrainment. In the section 7.1 & 7.2, the louvers were placed symmetrically with each other and the maximum diameter possible for such an arrangement was taken for flow computation.

However, to check the effect of changing angle between the louvers, the diameter of each hole was reduced as compared to previous section (7.1 and 7.2) by around 35%. This decreased the amount of mass flow through each hole, but provided ample space to vary the angle between the louvers for study. The mass flow rate computed in this section is different of those computed in section 7.1 & 7.2.
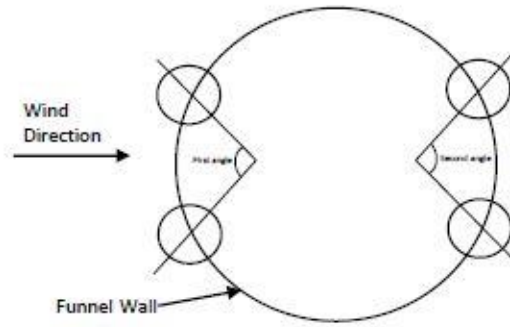

Figure 15: Angular placement of two adjacent louvers

Six louvers are taken in each row. If symmetrically placed around the central axis of the funnel, the angle between the louvers is 60°. The angle was reduced up to 40°. In figures 16 to 21, the legends show combination of two angles, for eg: 40-40, 50-50 etc. Figure 15 shows the detailed arrangement of louvers on the funnel wall. The first angle shows the placement of louvers on the funnel wall facing the wind direction and the second angle shows the placement on the opposite face of funnel wall. In the sub-sections below, the effect on mass suction ratio due to change in Reynolds number and change in wind velocity for different louver arrangement is shown.

7.3.1 Effect of changing Reynolds number.

The Reynolds number was varied for each angular arrangement and the variation of the mass suction ratio with the Reynolds number is shown. It can be seen from the graph that at lower angle combination i.e. 40° and 50° (asymmetrical placement) the mass suction is almost same and the curves are overlapping each other. But as we approach a symmetrical placement is 60°, the mass suction ratio is the maximum. Three wind velocities 2m/s, 6m/s and 10m/s were taken for study and the Reynolds number varied. As

we increase the Reynolds number, the mass suction ratio decreases which is in line with the trend as can be seen from the results in the previous section This true for all three wind velocities reported here.
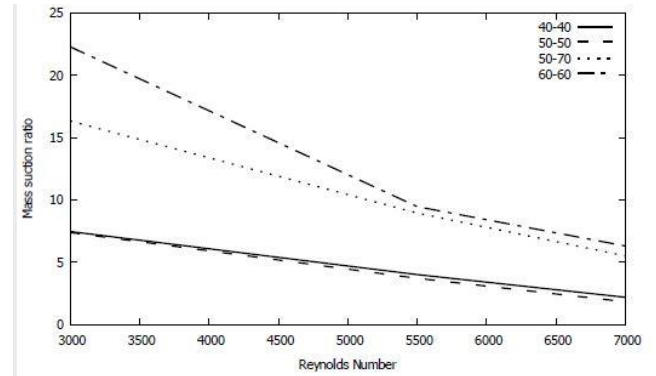
Figure 16: Wind velocity = 2 m/s
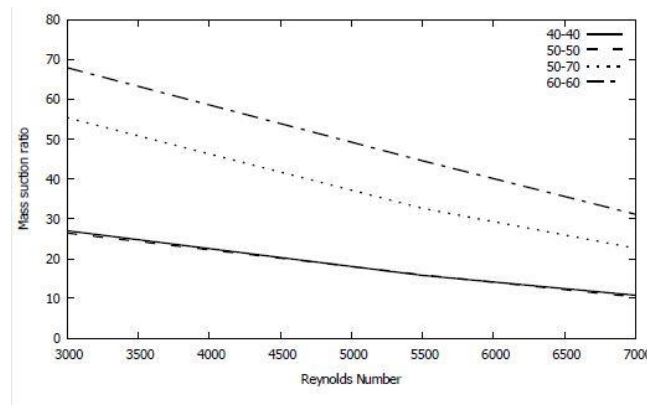
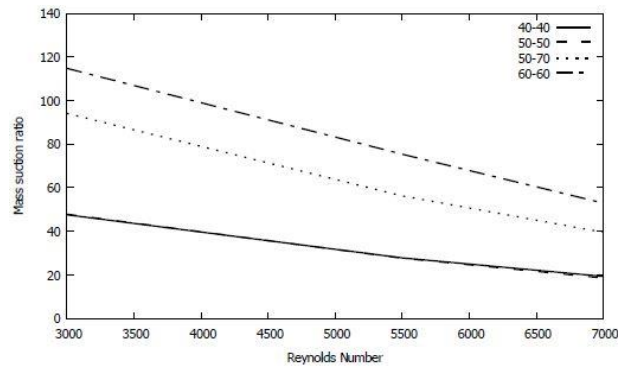
Figure 17: Wind Velocity = 6 m/s

Figure 18: Wind Velocity = 10 m/s

7.3.2 *Effect of varying wind velocity.*

The wind velocity was varied and the effect on the mass suction ratio was computed. It can be seen from the graph that at lower angle combination i.e. 40° and 50° (asymmetrical placement) the mass suction is almost same and the curves are overlapping each other. But as we approach a symmetrical placement is 60°, the mass suction ratio reaches to maximum value. Three values of nozzle exit Reynold\s number 3000, 5500 and 7000 were taken for study. It can be seen that with increasing wind velocity the mass suction ratio increases and shows a linear trend.
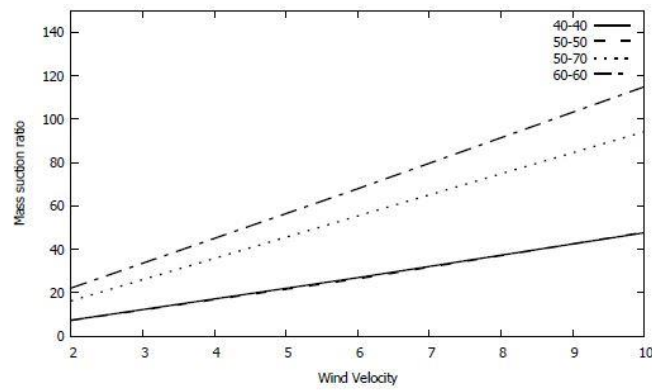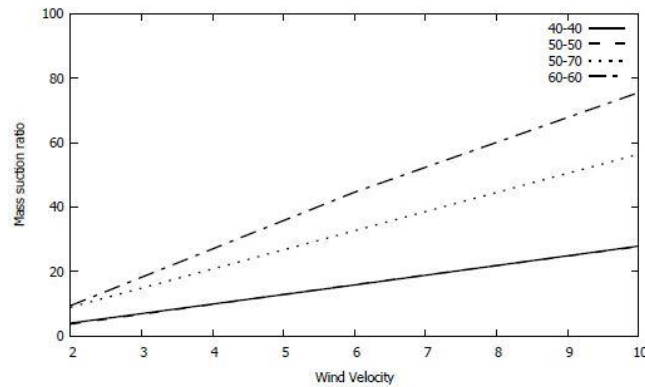

Figure 19: R_e = 3000
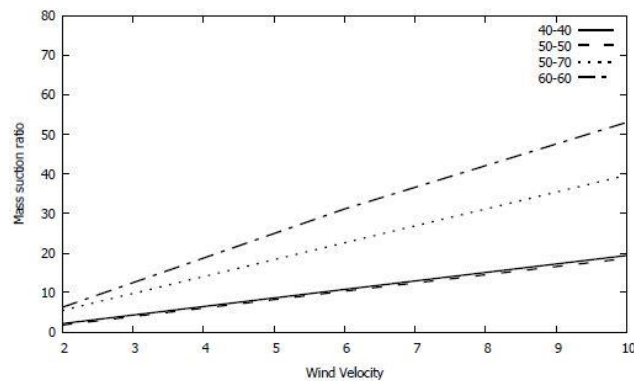

Figure 20: Re = 5500

Figure 21: Re = 7000

8. CONCLUSION

The variation of the nozzle exit Reynolds number has significant effect on the mass suction through the louvers. As the Reynolds number increases, for the same wind velocity, the mass suction decreases by almost 58% for rectangular placement of louvers and by 57% for triangular placement for whole range of Reynolds number studied. Numerical simulations show that there is a linear variation in the mass suction ratio when we increase the wind speed. The mass suction ratio increases with increase in wind speed. Lower Reynolds number and higher wind speed combination yields maximum mass suction ratio in the range studied. For triangular placement of louvers, the mass suction ratio decreases by about 8% across the range of Reynolds number So for maximum mass suction rectangular placement of louvers is suggested. When varying the angle between the louvers in each row, the symmetrical placement, irrespective of wind direction, is showing the highest mass suction ratio. As we bring the louvers closer, the mass suction ratio decreases. So equidistance/symmetrical placement of louvers is suggested.

ACKNOWLEDGEMENTS

REFERENCES

[1] Barik, A.K., Dash, S.K., Patro, P., Mohapatra, S. 2014. Experimental and numerical investigation of air entrainment into a louvred funnel. Applied Ocean Research, 48, pp. 176–185.

[2] Mishra, D.P., Dash, S.K. 2010. Numerical investigation of air suction through the louvers of a funnel due to high velocity air jet. Computers & Fluids, 39 (9), pp. 1597–1608.

[3] Sahu, S.R., Mishra, D.P. Open Ended Cylindrical Louvered Pipe. pp. 1–17.

[4] Sahu, S.R., Mishra, D.P. 2015. Effect of Pipe Configurations on Air Entrainment into a Louvered Cylindrical Pipe A Comparison between Open and Close Entrance of a Pipe. International Journal of Engineering Research, 5013 (4), pp. 173–177.

[5] Birk, A.M., VanDam, D. 1994. Infrared Signature Suppression for Marine Gas Turbines: Comparison of Sea Trial and Model Test Results for the DRES Ball IRSS System. Journal of Engineering for Gas Turbines and Power, 116 (1), p. 75.

[6] Ricou, F.P., Spalding, D.B. 1961. Measurements of entrainment by axisymmetric turbulent jets. Journal of Fluid Mechanics, 11 (1), 21-32.

[7] Pan, C., Zhang, J., Shan, Y. 2011. Modeling and analysis of helicopter thermal and infrared radiation. Chinese Journal of Aeronautics, 24 (5), pp. 558–567.

[8] Wang, S.F., Li, L.G. 2006. Investigations of flows in a new infrared suppressor. Applied Thermal Engineering, 26 (1), pp. 36–45.

[9] Ortega-Casanova, J., Granados-Ortiz, F.J. 2014. Numerical simulation of the heat transfer from a heated plate with surface variations to an impinging jet. International Journal of Heat and Mass Transfer, 76, pp. 128–143.

[10] Barik, A.K., Rout, S., Mukherjee, A. 2016. Numerical investigation of heat transfer enhancement from a protruded surface by cross-flow jet using Al2O3–water nanofluid. International Journal of Heat and Mass Transfer, 101, pp. 550–561.

[11] Mukherjee, A., Rout, S., Barik, A.K. 2016. Heat Transfer Enhancement from a Ribbed Surface in Presence of a Cross Flow Jet: A Numerical Investigation. Journal of Materials Science, 3 (3), pp. 172–178.

[12] Barik, A.K., Mukherjee, A., Patro, P. 2015. Heat transfer enhancement from a small rectangular channel with different surface protrusions by a turbulent cross flow jet. International Journal of Thermal Sciences, 98, pp. 32–41.

[13] Barik, A.K. 2015. Numerical investigation of heat transfer enhancement from a protruded surface by crossflow jet using Al2O3–water nanofluid. Applied Ocean Research, 101 (3), pp. 303–312.

[14] Barik, A.K., Dash, S.K., Guha, A. 2015. Entrainment of air into an infrared suppression (IRS) device using circular and non-circular multiple nozzles. Computers & Fluids, 114, pp. 26–38.

[15] Barik, A.K., Dash, S.K., Guha, A. 2014. New correlation for prediction of air entrainment into an Infrared Suppression (IRS) device. Applied Ocean Research, 47, pp. 303–312.

[16] Ansys R17.2, Ansys user manual.

NOMENCLATURE

D_f	:	Diameter of funnel
D_{nz}	:	Diameter of nozzle
L_p	:	Nozzle protrusion length
T_{nz}	:	Nozzle exit temperature
T_{sur}	:	Surrounding temperature
S_M	:	Sum of body forces
U	:	Velocity
C_μ	:	k-ε turbulence model constant
m_{suc}	:	Mass suction
m_{in}	:	Mass at nozzle inlet
μ_{eff}	:	Effective viscosity accounting to turbulence
μ	:	Dynamic Viscosity
μ_t	:	Turbulent Viscosity
ρ	:	Density
p'	:	Modified pressure.
k	:	Turbulence Kinetic Energy
ε	:	Turbulence Eddy dissipation rate